Mathematical and Computer Modelling 54 (2011) 210–220

Contents lists available at ScienceDirect

Mathematical and Computer Modelling

journal homepage: www.elsevier.com/locate/mcm

Finite difference schemes for multilayer diffusion

R.I. Hickson [a,b,*], S.I. Barry [a,b], G.N. Mercer [a,b], H.S. Sidhu [a]

[a] School of Physical, Environmental and Mathematical Sciences, University of New South Wales at ADFA, Northcott Drive, Canberra, ACT 2600, Australia
[b] National Centre for Epidemiology and Population Health, Australian National University, Canberra, ACT 0200, Australia

ARTICLE INFO

Article history:
Received 25 October 2010
Received in revised form 27 January 2011
Accepted 2 February 2011

Keywords:
Diffusion
Finite difference
Jump condition
Multilayer

ABSTRACT

Although numerical methods have been developed for diffusion through single layer materials, few have been developed for multiple layers. Diffusion processes through a multilayered material are of interest for a wide range of applications, including industrial, biological, electrical, and environmental areas. We present finite difference schemes for multilayered materials with a range of matching conditions between the layers, in particular for a jump matching condition. We show the finite difference methods are flexible, simple to implement, and help illustrate interesting behaviour in multilayered diffusion.

1. Introduction

Diffusion through multiple layers has applications to a wide range of areas in heat and mass transport. Industrial applications include annealing steel coils [1–3], the performance of semiconductors [4,5] and electrodes [6,7], geological profiles [8], and measuring greenhouse gas emission from soil surfaces [9]. Biological applications include determining the effectiveness of drug carriers inserted into living tissue [10], the probing of biological tissue with infrared light [11], and analysing the heat production of muscle [12].

For multilayer diffusion across n layers the standard linear diffusion equation,

$$\frac{\partial U_i}{\partial t} = D_i \frac{\partial^2 U_i}{\partial x^2}, \quad i = 1, 2, \ldots, n, \tag{1}$$

is applicable in each layer, where $x_{i-1} \le x \le x_i$ is the distance within layer i, $U_i(x, t)$ is the concentration of the diffusing substance in layer i at time t, and D_i is the diffusivity of layer i, as shown in Fig. 1. For simplicity throughout this paper the diffusing quantity is taken to be heat and hence we refer to temperature and heat flux.

Finite difference schemes are common for diffusion through a single layer (see for example [13]). However, considerably less work has been done developing finite difference schemes involving multiple layers. Notably, Iliev [14] uses an averaging of the diffusivities across the interface; Wiegmann and Bube [15] use a Taylor series to find corrections for the standard scheme for a jump condition across the interface; Xue and Deng [16] use 'ghost points' around the interface and Taylor series approximations to produce a finite difference scheme for Maxwell's equations; and Wang [17] uses tensors in a curvilinear coordinate system to develop a finite difference scheme.

In this article, we develop various finite difference schemes suitable for multilayered diffusion and different matching conditions at interfaces $x = x_i$, $i = 1, 2, \ldots, (n-1)$, as shown in Fig. 1. The schemes developed here are useful for research questions concerning diffusion through multiple layers. In Hickson et al. [18], we found exact solutions for diffusion through

* Corresponding author at: National Centre for Epidemiology and Population Health, Australian National University, Canberra, ACT 0200, Australia. Tel.: +61 2 6125 0446; fax: +61 6125 0740.
E-mail addresses: RI.Hickson@gmail.com, Roslyn.Hickson@anu.edu.au (R.I. Hickson).

0895-7177/$ – see front matter
doi:10.1016/j.mcm.2011.02.003

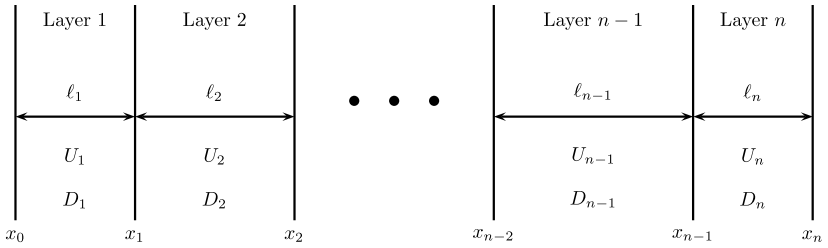

Fig. 1. Multilayer schematic, where $U_i(x, t)$ is the concentration of the diffusing substance in layer i at time t, D_i is the diffusivity of layer i, x is the distance and x_i the layer interface, and ℓ_i is the layer width.

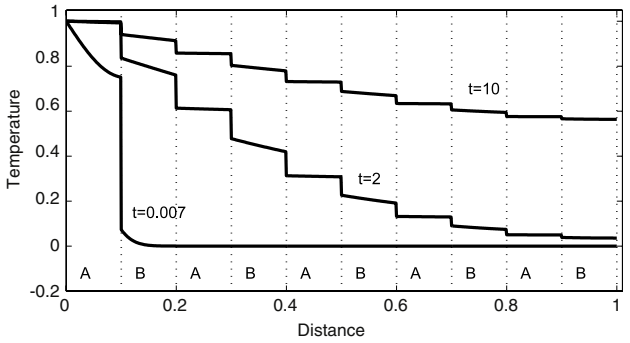

Fig. 2. Temperature profiles for a 10 layer region, with diffusivities in the 'A' layers $D_A = 1$, for the 'B' layers $D_B = 0.1$, $(a_1, b_1) = (1, 0), \theta_1 = 1$, $(a_2, b_2) = (0, 1), \theta_2 = 0$, $\ell_i = 0.1$, and $H_i = 0.5$, at times $t = 0.007, 2, 10$.

single and multiple layers. The exact solutions were verified against numerical solutions found using the methods described in Sections 2–5.

An important aspect of layered materials is the matching conditions at the interfaces, where an 'interface' is the common boundary between two layers. There are three different matching conditions of particular interest. The first matching conditions assume continuity in 'temperature' and flux at the interfaces, $x = x_i$, such that

$$U_i(x_i, t) = U_{i+1}(x_i, t), \tag{2}$$

$$D_i \left.\frac{\partial U_i}{\partial x}\right|_{x_i} = D_{i+1} \left.\frac{\partial U_{i+1}}{\partial x}\right|_{x_i}, \tag{3}$$

where D_i and D_{i+1} are the diffusivities in layers i and $i + 1$ respectively. This matching condition is considered in Section 2.

The second matching condition is with respect to the conductivities, κ_i, as opposed to the diffusivities in Eq. (3):

$$\kappa_i \left.\frac{\partial U_i}{\partial x}\right|_{x_i} = \kappa_{i+1} \left.\frac{\partial U_{i+1}}{\partial x}\right|_{x_i}, \tag{4}$$

where $\kappa_i = \rho_i c_i D_i$. This is the more general version of Eq. (3), and is applicable when the density, ρ_i, and specific heat capacity, c_i, are possibly different in each layer. In fact, Eqs. (3) and (4) highlight the key difference between heat and mass transport problems, as Eq. (3) expresses equality of mass flux and Eq. (4) expresses equality of heat flux. This matching condition is considered in Section 3.

The third matching condition is considered in Section 4, and extends Eq. (4) to use jump conditions where

$$\begin{aligned} \kappa_i \frac{\partial U_i}{\partial x} &= H_i \left(U_{i+1} - U_i\right), \\ \kappa_{i+1} \frac{\partial U_{i+1}}{\partial x} &= H_i \left(U_{i+1} - U_i\right), \end{aligned} \tag{5}$$

and H_i is the contact transfer coefficient. This matching condition is more general than Eq. (4), as it models roughness of the contact between the layers [1] and contact resistance [19] at the interfaces. If $H_i \to \infty$, then contact becomes perfect and hence this limit represents the equivalent matching conditions from Eqs. (2) and (4). The imperfect contact is depicted in Fig. 2 using temperature profiles, clearly demonstrating the 'jump' at the interfaces. This figure shows temperature, U, as a function of distance $x \in [0, 1]$ at three different times.

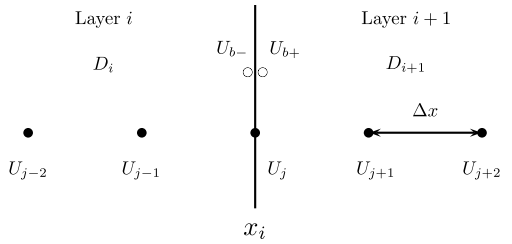

Fig. 3. Schematic diagram of the grid-points (dots) and the finite difference scheme indexing, where i denotes the layer, j denotes the spatial discretization, and $b\pm$ denote the points slightly to the positive (right) or negative (left) sides of the interface.

For completeness, Section 5 determines the finite difference scheme at the outer boundaries, for general mixed boundary conditions:

$$\begin{aligned} a_1\, U_1 + b_1\, \frac{\partial U_1}{\partial x} &= \theta_1, \quad \text{at} \quad x = x_0, \\ a_2\, U_n + b_2\, \frac{\partial U_n}{\partial x} &= \theta_2, \quad \text{at} \quad x = x_n. \end{aligned} \tag{6}$$

For comparison to an exact solution, a two-layer case study is considered in Section 6. The exact solution is first outlined in Section 6.1, and the accuracy of the finite difference schemes from Sections 2 and 4 are depicted in Section 6.2. Finally, these results are discussed in Section 7.

2. Matching diffusivities

This section considers the first matching conditions, Eqs. (2) and (3), assuming continuity in temperature and flux at the interfaces. The analysis in this section assumes one grid-point lies on the interface for the spatial discretization. Fig. 3 depicts an interface between layers with the nomenclature and indexing used in this section.

Consider the diffusion equation through multiple layers:

$$\frac{\partial U_i}{\partial t} = \frac{\partial}{\partial x}\left(D_i \frac{\partial U_i}{\partial x}\right), \tag{7}$$

with matching conditions

$$\begin{aligned} U_{b-} &= U_{b+}, \\ D_i \frac{\partial U_{b-}}{\partial x} &= D_{i+1} \frac{\partial U_{b+}}{\partial x}, \end{aligned} \tag{8}$$

at the interfaces, $x = x_i$. The inner points of a layer use the standard first-order time and second-order space finite differencing. That is, the space finite differencing at point $(j-1)$ gives

$$\frac{\partial U_{j-1}}{\partial t} = \frac{D_i \left(U_{j-2} - 2U_{j-1} + U_j\right)}{\Delta x^2}, \tag{9}$$

where U_{j-1} is the temperature at the spatial point $(j-1)$ in layer i.

For the point on the interface, taking a central difference for Eq. (7) gives

$$\frac{\partial U_j}{\partial t} = \frac{D_{i+1} \frac{\partial U_{b+}}{\partial x} - D_i \frac{\partial U_{b-}}{\partial x}}{\Delta x}. \tag{10}$$

First-order forward and backward differences for the spatial derivative then give:

$$\begin{aligned} \frac{\partial U_j}{\partial t} &= \frac{D_{i+1}\left(\frac{U_{j+1}-U_j}{\Delta x}\right) - D_i\left(\frac{U_j - U_{j-1}}{\Delta x}\right)}{\Delta x} \\ &= \frac{D_{i+1}\, U_{j+1} - (D_{i+1} + D_i) U_j + D_i\, U_{j-1}}{\Delta x^2}. \end{aligned} \tag{11}$$

Thus the differencing for this system can be illustrated by the following matrix

$$\frac{\mathrm{d}}{\mathrm{d}t}\begin{bmatrix}\vdots\\ U_{j-2}\\ U_{j-1}\\ U_j\\ U_{j+1}\\ U_{j+2}\\ \vdots\end{bmatrix}=\begin{bmatrix}\ddots & & & & & & \\ & \ddots & & & & & \\ \cdots & \chi_i & -2\chi_i & \chi_i & 0 & 0 & \cdots\\ \cdots & 0 & \chi_i & -\chi_i-\chi_{i+1} & \chi_{i+1} & 0 & \cdots\\ \cdots & 0 & 0 & \chi_{i+1} & -2\chi_{i+1} & \chi_{i+1} & \cdots\\ & & & & \ddots & & \\ & & & & & \ddots & \end{bmatrix}\begin{bmatrix}\vdots\\ U_{j-2}\\ U_{j-1}\\ U_j\\ U_{j+1}\\ U_{j+2}\\ \vdots\end{bmatrix}, \tag{12}$$

where $\chi_i = D_i/\Delta x^2$, and $\chi_{i+1} = D_{i+1}/\Delta x^2$. Eq. (12) is easily extended to multiple layers with numerous internal points and any boundary conditions. This can then be iterated in time using standard integration routines such as Euler time stepping. For example

$$\mathbf{U}(t+\Delta t) = \mathbf{U}(t) + \Delta t\ \boldsymbol{\chi}\ \mathbf{U}(t). \tag{13}$$

Here $\mathbf{U}$ and $\boldsymbol{\chi}$ are the obvious vector and matrix notations of Eq. (12).

3. Matching conductivities

The scheme outlined in Section 2 implicitly assumes continuity in temperature and flux across the interfaces using the diffusivity matching condition, Eq. (3). However, for heat transfer problems, the more general conductivity matching condition, Eq. (4), is applicable. In this section a suitable finite difference scheme is developed which explicitly incorporates the matching conductivity. It assumes the matching point lies on the interface.

The main differences between this scheme and that described in Section 2 are the use of conductivities, κ_i, for the matching condition, and the explicit use of the matching condition around the fictitious points U_{b-} and U_{b+}, as shown in Fig. 3. Since continuity, $U_{b-} = U_{b+}$, is assumed at the interface, let the flux be the average of the fluxes at the two fictitious matching points. That is,

$$D_j\frac{\partial^2 U_j}{\partial x^2} = \frac{1}{2}\left(D_i\frac{\partial^2 U_{b-}}{\partial x^2} + D_{i+1}\frac{\partial^2 U_{b+}}{\partial x^2}\right), \tag{14}$$

hence expressions for $\partial^2 U_{b-}/\partial x^2$ and $\partial^2 U_{b+}/\partial x^2$ must be found.

Taylor series approximations are taken for U_{j-1}, U_{j-2}, U_{j+1} and U_{j+2} in terms of U_{b-} and U_{b+} respectively:

$$\begin{aligned}
U_{j-1} &\approx U_{b-} - \Delta x\frac{\partial U_{b-}}{\partial x} + \frac{\Delta x^2}{2}\frac{\partial^2 U_{b-}}{\partial x^2},\\
U_{j-2} &\approx U_{b-} - 2\Delta x\frac{\partial U_{b-}}{\partial x} + 2\Delta x^2\frac{\partial^2 U_{b-}}{\partial x^2},\\
U_{j+1} &\approx U_{b+} + \Delta x\frac{\partial U_{b+}}{\partial x} + \frac{\Delta x^2}{2}\frac{\partial^2 U_{b+}}{\partial x^2},\\
U_{j+2} &\approx U_{b+} + 2\Delta x\frac{\partial U_{b+}}{\partial x} + 2\Delta x^2\frac{\partial^2 U_{b+}}{\partial x^2}.
\end{aligned} \tag{15}$$

These, combined with Eqs. (2) and (4) give six equations with six unknowns. Solving them using Maple [20] subsequently yields

$$\begin{aligned}
\frac{\partial^2 U_{b-}}{\partial x^2} &\approx \frac{(2\,\kappa_i + 3\,\kappa_{i+1})\,U_{j-2} - (2\,\kappa_i + 6\,\kappa_{i+1})\,U_{j-1} + 4\,\kappa_{i+1}\,U_{j+1} - \kappa_{i+1}\,U_{j+2}}{3\,(\kappa_i + \kappa_{i+1})\,\Delta x^2},\\
\frac{\partial^2 U_{b+}}{\partial x^2} &\approx \frac{-\kappa_i\,U_{j-2} + 4\,\kappa_i\,U_{j-1} - (6\,\kappa_i + 2\,\kappa_{i+1})\,U_{j+1} + (3\,\kappa_i + 2\,\kappa_{i+1})\,U_{j+2}}{3\,(\kappa_i + \kappa_{i+1})\,\Delta x^2}.
\end{aligned} \tag{16}$$

Substituting these into Eq. (14) gives

$$\begin{aligned}
D_i\frac{\partial^2 U_j}{\partial x^2} \approx\ & \Upsilon_i\Big\{[(2\,\kappa_i + 3\,\kappa_{i+1})\,D_i - D_{i+1}\,\kappa_i]\ U_{j-2} + [-2(\kappa_i + 3\,\kappa_{i+1})\,D_i + 4\,D_{i+1}\,\kappa_i]\ U_{j-1}\\
&+ [4\,D_i\,\kappa_{i+1} - 2(3\,\kappa_i + \kappa_{i+1})\,D_{i+1}]\ U_{j+1} + [-D_i\,\kappa_{i+1} + (3\,\kappa_i + 2\,\kappa_{i+1})\,D_{i+1}]\ U_{j+2}\Big\},
\end{aligned} \tag{17}$$

where $\Upsilon_i = 1/[6\,(\kappa_i + \kappa_{i+1})\,\Delta x^2]$. Again, using standard central differencing for points not at the interface results in the same type of matrix as in Eq. (12) (which is not shown for brevity) with the middle row replaced with the relevant terms from Eq. (17). As done previously, this can then be iterated in time using standard Euler time stepping or other methods.

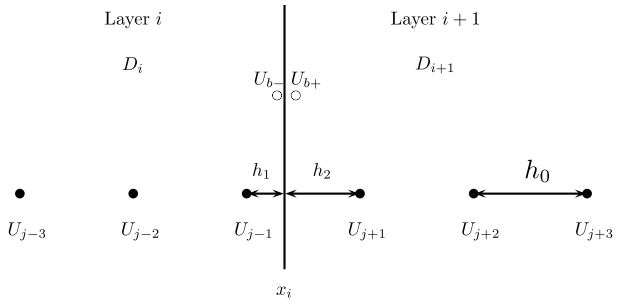

Fig. 4. Finite difference scheme indexing, where i denotes the layer, j denotes the spatial discretization, and $b\pm$ denote the points slightly to the positive (right) or negative (left) sides of the interface. h_0 is the distance between the inner spatial discretization, h_1 is the distance between U_{j-1} and the interface, and h_2 is the distance between the interface and U_{j+1}.

4. Jump matching condition

The finite difference scheme outlined in Section 3 explicitly takes into account the condition at the interface, and is extendable to the jump condition, Eq. (5). Due to the jump across the interface, there is no single value and hence it is assumed there is no grid-point on the interface, as depicted in Fig. 4. This immediately implies that Eq. (14) no longer holds. A combination of the methods used in Sections 2 and 3 are used to find $\partial^2 U_{b-}/\partial x^2$ and $\partial^2 U_{b+}/\partial x^2$ in terms of the fictitious points U_{b-} and U_{b+}, and expressions for U_{b-} and U_{b+} respectively.

The second derivatives are found using a central difference approximation and then forwards and backwards differences give

$$\begin{aligned}
\frac{\partial^2 U_{j-1}}{\partial x^2} &\approx \frac{h_0\, U_{b-} - (h_0+h_1)U_{j-1} + h_1\, U_{j-2}}{h_0\, h_1\, (h_0+h_1)},\\
\frac{\partial^2 U_{j+1}}{\partial x^2} &\approx \frac{h_2\, U_{j+2} - (h_0+h_2)U_{j+1} + h_0\, U_{b+}}{h_0\, h_2\, (h_0+h_2)},
\end{aligned} \tag{18}$$

where the subscripts are explained in Fig. 4. When $h_0 = h_1 = h_2 = \Delta x$, these become the standard finite differences, as in Eq. (9).

The expressions for U_{b-} and U_{b+} are found using Taylor series around U_{j-1}, U_{j-2}, U_{j+1} and U_{j+2} in terms of U_{b-} and U_{b+} respectively, as done in Section 3:

$$\begin{aligned}
U_{j-1} &\approx U_{b-} - h_1 \frac{\partial U_{b-}}{\partial x} + \frac{h_1^2}{2}\frac{\partial^2 U_{b-}}{\partial x^2},\\
U_{j-2} &\approx U_{b-} - (h_0+h_1)\frac{\partial U_{b-}}{\partial x} + \frac{(h_0+h_1)^2}{2}\frac{\partial^2 U_{b-}}{\partial x^2},\\
U_{j+1} &\approx U_{b+} + h_2 \frac{\partial U_{b+}}{\partial x} + \frac{h_2^2}{2}\frac{\partial^2 U_{b+}}{\partial x^2},\\
U_{j+2} &\approx U_{b+} + (h_0+h_2)\frac{\partial U_{b+}}{\partial x} + \frac{(h_0+h_2)^2}{2}\frac{\partial^2 U_{b+}}{\partial x^2}.
\end{aligned} \tag{19}$$

As before, there are six equations for six unknowns.[1] Using Maple, these yield expressions for the fictitious points U_{b-} and U_{b+} as

$$\begin{aligned}
U_{b-} \;\approx\; & \frac{1}{\Lambda_i}\Big\{\left[-((h_0+h_2)(h_2\,H_i+\kappa_{i+1})+h_2\,\kappa_{i+1})\,h_1^2\,\kappa_i\right]\,U_{j-2}\\
&+\left[((h_0+h_2)\,(h_2\,H_i+\kappa_{i+1})+h_2\,\kappa_{i+1})\,(h_0+h_1)^2\,\kappa_i\right]\,U_{j-1}\\
&+\left[h_1(h_0+h_1)(h_0+h_2)^2\,H_i\,\kappa_{i+1}\right]\,U_{j+1}+\left[-h_1\,h_2^2\,(h_0+h_1)\,H_i\,\kappa_{i+1}\right]\,U_{j+2}\Big\},\\
U_{b+} \;\approx\; & \frac{1}{\Lambda_i}\Big\{\left[-h_1^2\,h_2(h_0+h_2)H_i\,\kappa_i\right]\,U_{j-2}+\left[h_2(h_0+h_1)^2(h_0+h_2)H_i\,\kappa_i\right]\,U_{j-1}\\
&+\left[((h_0+h_1)(h_1\,H_i+\kappa_i)+h_1\,\kappa_i)(h_0+h_2)^2\,\kappa_{i+1}\right]\,U_{j+1}\\
&+\left[-((h_0+h_1)(h_1\,H_i+\kappa_i)+h_1\,\kappa_i)\,h_2^2\,\kappa_{i+1}\right]\,U_{j+2}\Big\},
\end{aligned} \tag{20}$$

[1] It is also possible to ignore the last two series and the second-order terms and find a simpler, first-order, approximation for U_{b-} and U_{b+}.

where

$$\Lambda_i = h_0 \{[(h_0 + 2h_1)(h_0 + h_2)h_2\kappa_i + (h_0 + h_1)(h_0 + 2h_2)h_1\kappa_{i+1}]\, H_i + (h_0 + 2h_1)(h_0 + 2h_2)\kappa_i\kappa_{i+1}\}\,. \tag{21}$$

In the particular case when $h_0 = h_1 = h_2 = \Delta x$ and $H_i \to \infty$, the combination of Eqs. (18), (20) and (21) give $\frac{\partial^2 U_{j-1}}{\partial x^2} = \frac{\partial^2 U_{b-}}{\partial x^2}$ and $\frac{\partial^2 U_{j+1}}{\partial x^2} = \frac{\partial^2 U_{b+}}{\partial x^2}$ from Section 3, Eq. (16), and hence reduce to the more straightforward case. The numerical implementation thus uses the two fictitious points and the standard Euler time stepping procedure.

5. Mixed boundary conditions

For completeness, in this section we demonstrate how the boundary conditions are incorporated into the finite difference schemes outlined in Sections 2–4. Using fictitious points U_{-1} and U_{n+1} a distance Δx from the $x = x_0$ and $x = x_n$ boundaries respectively, it can be shown that

$$\frac{\mathrm{d}U_0}{\mathrm{d}t} = \frac{1}{\Delta x^2}\left[2U_1 + 2U_0\left(\frac{a_1\Delta x}{b_1} - 1\right)\right] - \frac{2\theta_1}{b_1\Delta x}, \tag{22}$$

$$\frac{\mathrm{d}U_n}{\mathrm{d}t} = \frac{1}{\Delta x^2}\left[2U_{n-1} - 2U_n\left(\frac{a_2\Delta x}{b_2} + 1\right)\right] + \frac{2\theta_2}{b_2\Delta x}. \tag{23}$$

This scheme in combination with schemes from Sections 2–4 are used to verify the exact solutions found in Hickson et al. [18,21,22].

6. Two layer example

This section considers diffusion through two layers to illustrate the effectiveness of the finite difference schemes from Sections 2 and 4. Two layers are useful for a large variety of applications [4,9,10,23–26].

This section is divided into two parts. The exact solution for two layers using a jump matching condition is briefly outlined in Section 6.1, and is based on the solutions presented in Hickson et al. [18,21,22]. Results indicating the accuracy of the finite difference schemes are depicted in Section 6.2.

6.1. Exact solution

The system is governed by Eq. (1), with $i = 1$ corresponding to the domain $x \in [x_0, x_1]$ and $i = 2$ corresponding to $x \in [x_1, x_2]$. The boundary conditions are similar to those in Eq. (6), but here for the sake of brevity we use one fixed temperature boundary ($x = x_0$) and one mixed boundary ($x = x_2$):

$$\begin{aligned} &U_1(x_0, t) = 1, \\ &a\,U_2 + b\,\frac{\partial U_2}{\partial x} = \theta, \quad \text{at} \quad x = x_2. \end{aligned} \tag{24}$$

More general boundary conditions are, of course, possible. The initial condition is $U_i(x, 0) = f_i(x) = 0$. The interface conditions are the jump conditions from Eq. (5):

$$\begin{aligned} \kappa_1\frac{\partial U_1}{\partial x} &= H\,(U_2 - U_1)\,, \\ \kappa_2\frac{\partial U_2}{\partial x} &= H\,(U_2 - U_1)\,. \end{aligned} \tag{25}$$

The solution is found by separating the problem into the steady state, $w_i(x)$, and transient components, $v_i(x, t)$, for $i = 1, 2$. Separation of variables is then used for the transient component such that $v_i(x, t) = X_i(x)T(t)$. The two layer solution is then written as

$$U_i(x, t) = w_i(x) + \sum_{m=1}^{\infty} C_m \mathrm{e}^{-\lambda_m^2 t} X_{i,m}(x). \tag{26}$$

Using the boundary and matching conditions, the steady state solutions are

$$\begin{aligned} w_1 &= 1 - \frac{\kappa_2\, H(a - \theta)\, x}{b\,\kappa_1\, H + a\,\kappa_2\,\ell_1\, H + a\,\kappa_1\,\ell_2\, H + a\,\kappa_1\,\kappa_2}, \\ w_2 &= 1 - \frac{(a - \theta)\,[\kappa_1\, H(x - x_1) + \kappa_2(\ell_1\, H + \kappa_1)]}{b\,\kappa_1\, H + a\,\kappa_2\,\ell_1\, H + a\,\kappa_1\,\ell_2\, H + a\,\kappa_1\,\kappa_2}, \end{aligned} \tag{27}$$

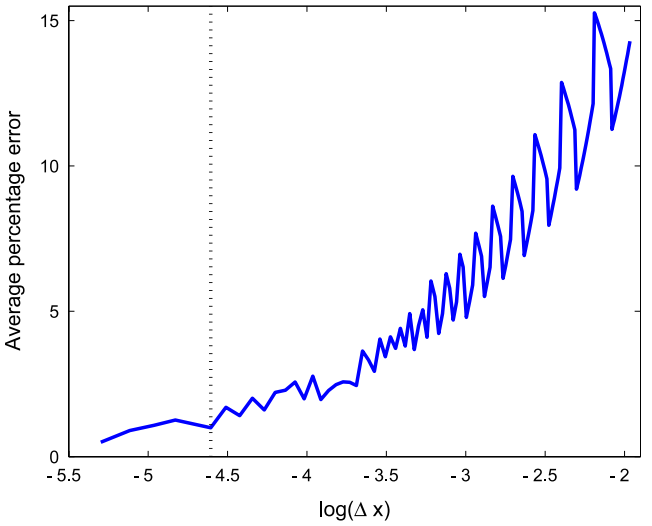

Fig. 5. Average percent error of the finite difference solution as a function of the spatial discretization, $\log_e(\Delta x)$. Here $D_1 = 1$, $D_2 = 0.1$, $t = 1$, using the first fifty eigenvalues of the analytical solution in the summations.

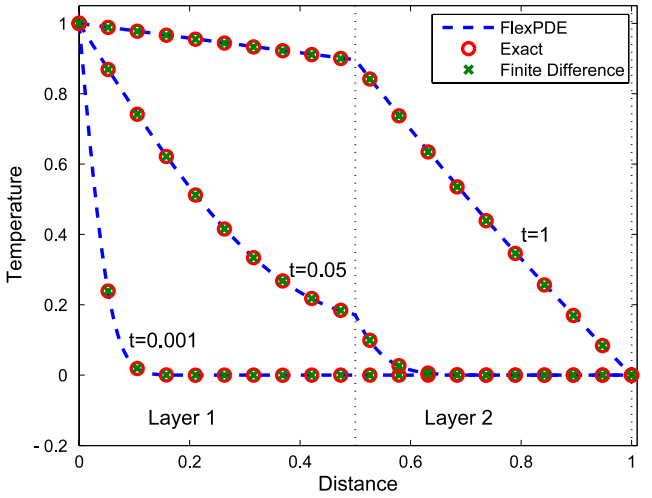

Fig. 6. Temperature as a function of distance for the three implementations: the exact solution, Eq. (26); the finite difference scheme from Section 2; and the finite elements solution using the commercial package FlexPDE [28]. Here $D_1 = 1$, $D_2 = 0.1$, $\Delta x = 0.01$, using the first fifty eigenvalues of the analytical solution in the summations.

where w_1 is the steady state solution in layer one, w_2 is the steady state in layer two [18,22]. The summation coefficient is found using Sturm–Liouville theory:

$$C_m = \frac{\sum_{i=1}^{n} \rho_i\, c_i \int_{x_{i-1}}^{x_i} g_i(x) X_{i,m}(x)\, \mathrm{d}x}{\sum_{i=1}^{n} \rho_i\, c_i \int_{x_{i-1}}^{x_i} X_{i,m}^2(x)\, \mathrm{d}x}, \tag{28}$$

where $g_i(x) = f_i(x) - w_i(x)$. The eigenfunctions are

$$X_{i,m}(x) = J_{i,m} \sin\left(\frac{\lambda_m}{d_i}(x - x_{i-1})\right) + K_{i,m} \cos\left(\frac{\lambda_m}{d_i}(x - x_{i-1})\right), \tag{29}$$

where the coefficients of the eigenfunctions are $J_{1,m} = 1$, $K_{1,m} = 0$,

$$J_{2,m} = \frac{\kappa_1\, d_2}{\kappa_2\, d_1} \cos\left(\lambda_m \frac{\ell_1}{d_1}\right), \tag{30}$$

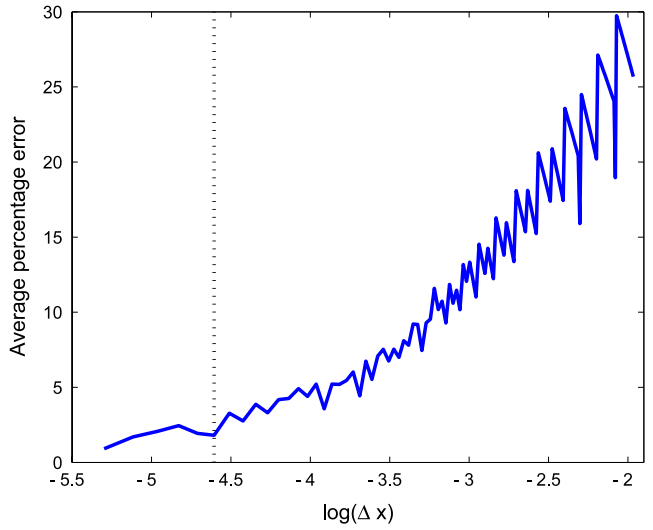

Fig. 7. Average percent error of the finite difference solution as a function of the spatial discretization, $\log_e(\Delta x)$. Here $D_1 = 1, D_2 = 0.1, t = 1, H = 0.5$, using the first fifty eigenvalues of the analytical solution in the summations.

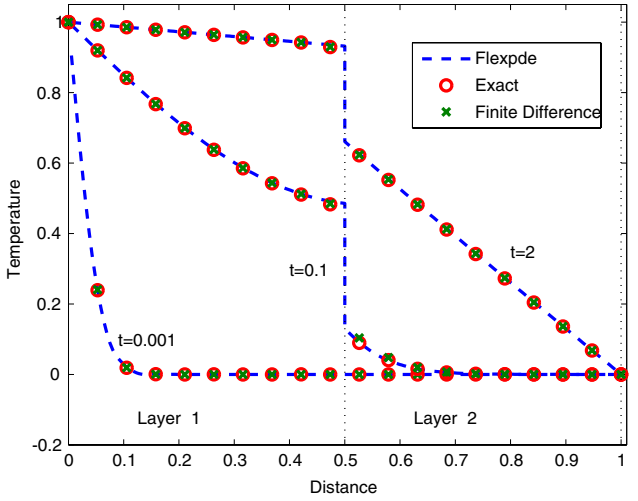

Fig. 8. Temperature as a function of distance for the three implementations: the exact solution, Eq. (26); the finite difference scheme from Section 2; and the finite elements solution using the commercial package FlexPDE [28]. Here $D_1 = 1, D_2 = 0.1, \Delta x = 0.01, H = 0.5$, using the first fifty eigenvalues of the analytical solution in the summations.

$$K_{2,m} = \sin\left(\lambda_m \frac{\ell_1}{d_1}\right) + \frac{\kappa_1 \lambda_m}{d_1 H} \cos\left(\lambda_m \frac{\ell_1}{d_1}\right). \tag{31}$$

The eigenvalues, λ_m, are defined by the transcendental expression

$$J_{2,m}\left[a \sin\left(\lambda_m \frac{\ell_2}{d_2}\right) + \frac{\lambda_m b}{d_2} \cos\left(\lambda_m \frac{\ell_2}{d_2}\right)\right] + K_{2,m}\left[-\frac{\lambda_m b}{d_2} \sin\left(\lambda_m \frac{\ell_2}{d_2}\right) + a \cos\left(\lambda_m \frac{\ell_2}{d_2}\right)\right] = 0. \tag{32}$$

6.2. Accuracy of the schemes

The analytical solution, Eq. (26), is verified using our finite difference schemes implemented in MATLAB [27], and also checked using the commercial finite elements package FlexPDE [28]. The results in Section 6.2.1 use the finite difference scheme from Section 2, for matching flux and diffusivity at the interfaces. The results in Section 6.2.2 consider the jump

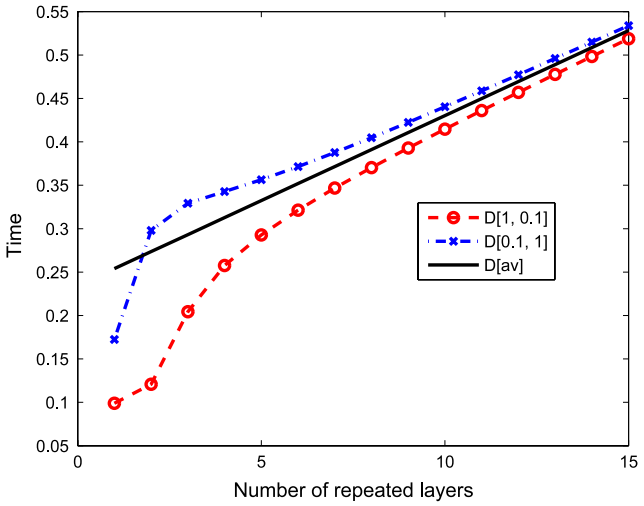

Fig. 9. Critical time as a function of number of repeated layers, n. Here $\ell_i = 1/n$ such that $\sum \ell_i = 1$, $(a_1, b_1) = (1, 0)$ and $(a_2, b_2) = (1, 0)$, $\theta_1 = 1$ and $\theta_2 = 0$, and $H_i = 5$. Diffusivities are repeated as either $D = 1, 0.1, 1, 0.1 \ldots$ ('D[1, 0.1]'), $D = 0.1, 1, 0.1, 1, \ldots$ ('D[0.1, 1]'), or D[av] $= 1/\left(\sum \ell_i/D_i + \sum 1/H_i\right)$.

finite difference scheme from Section 4. In both cases, the results were determined using $a = 1$, $b = 0$, and $\theta = 0$ for Eq. (24); and $\kappa = D$ for Eq. (25).

6.2.1. Matching flux and diffusivity

Fig. 5 depicts the average relative error of the analytical solution versus the numerical finite difference scheme for two layers at $t = 1$, where $H \to \infty$ and hence Eq. (3) and the finite difference scheme from Section 2 are used. The percentage error is

$$\%\,\text{Error}(x) = \frac{U_i(x, t) - U_{\text{fds}}(x, t)}{U_i(x, t)} \times 100\%, \tag{33}$$

where $U_i(x, t)$ is the analytical solution, Eq. (26) using the first fifty terms in the summation, and $U_{\text{fds}}(x, t)$ is the solution using the finite difference scheme from Section 2. Since the error is dependent on the distance, x, the average percentage error is plotted. The trade-off in choosing the spatial discretization is between computational efficiency and accuracy. For example, for $\Delta x = 0.005$, the finite difference scheme took 25.7 s, whereas for $\Delta x = 0.14$, it took 0.001 of a second, on a standard PC (3.2 GB RAM, 3 GHz Intel Core 2 Duo CPU). The vertical black dotted line depicts the spatial discretization used for results shown in Fig. 6. Smaller discretizations show identical behaviour and the accuracy improvement is marginal.

Fig. 6 depicts the numerically implemented analytical solution ('Exact') (red circles) against the finite elements solution using FlexPDE [28] (blue dashed line), and the MATLAB [27] finite difference scheme outlined in Section 2 (green crosses). The spatial discretization used is $\Delta x = 0.01$, which corresponds to the vertical black dotted line in Fig. 5, and fifty terms were used in the summation. The agreement between the numerical and analytical solutions are found to within the expected numerical accuracy. Furthermore, the codes were tested by setting the diffusivities equal for both layers, whereby the single layer solutions are recovered.

6.2.2. Jump matching condition

To demonstrate the difference in accuracy between the finite difference schemes, this section considers the jump matching condition scheme from Section 4, where $H = 0.5$ in Eq. (25).

Fig. 7 depicts the mean relative error between the numerically implemented analytical ('Exact') solution and the finite difference scheme, as per Eq. (33), as the discretization is changed. The main difference between Figs. 5 and 7 is the level of inaccuracy of the jump finite difference scheme with increasing spatial discretization size. That is, $\approx 30\%$ at $\log_e(\Delta x) = -2$ for Fig. 7 versus $\approx 15\%$ for Fig. 5. This is expected as more points are required to capture the jumps across the interface(s). However, when a suitable discretization is chosen, the schemes are just as accurate, with less than 5% relative error for the values used here.

Fig. 8 depicts the difference between the three implementations for the 'Temperature' profiles, as done in Fig. 6 for the continuous matching condition. The jump finite difference scheme is less accurate than the continuous scheme at smaller times, but is still within expected numerical accuracy. The spatial discretization used here is $\Delta x = 0.01$, as for the previous case, which corresponds to the vertical black dotted line in Fig. 7. Furthermore, the code was tested by setting $H = 1000$ to approximate no contact resistance ($H \to \infty$), and the results from Section 6.2.1 were recovered.

7. Discussion and conclusions

The main advantages of the finite difference schemes outlined in this paper are that they are easy to implement, and are flexible for exploring various research questions involving problems where a quantity is diffusing through multiple layers. Such problems are important in science, engineering, and medical applications [2,4,10].

To illustrate the ease of implementation and flexibility of our numerical schemes, we used them, along with the analytic solutions to successfully examine the question "how long do diffusion transport processes take through layered materials?" (see [18,21,22,29–31]). This question is of interest in a variety of fields (see for example [32,33]). This involves inverting the solutions, both analytical and numerical, to find the time it takes to fulfil a particular criterion, such as the time when the temperature reaches a critical value. Fig. 9 demonstrates the effect multiple layers have on such a critical time definition, in this instance when the average temperature reaches half the average steady state (see Hickson et al. [18], Equation (2)). The blue dot-dashed line with crosses depicts the critical time when the diffusivities are repeated in the layers as $D = 0.1, 1, 0.1, 1, \ldots$, referred to as a biperiodic region. The red dashed line with circles similarly depicts the critical time when the biperiodic ordering is reversed, so $D = 1, 0.1, 1, 0.1, \ldots$, and the black solid line represents the diffusivities being averaged across the region as $D = 1/\left(\sum \ell_i/D_i + \sum 1/H_i\right)$. Hence Fig. 9 demonstrates how the layer order effects the critical time, as well as the number of layers.

The analytical 'exact' solution is more accurate and less computationally intensive, at least for the two layer case. However, the 'exact' solution is not always able to be found through analytical means, and for multiple layers numerical integration techniques are often required. Whereas, the finite difference schemes outlined in this paper are straightforward to implement for differing problems, and are hence more flexible.

References

[1] S. Barry, W. Sweatman, Modelling heat transfer in steel coils, ANZIAM Journal(E) 50 (2009) C668–C681.
[2] M. McGuinness, W. Sweatman, D. Boawan, S. Barry, Annealing steel coils, in: T. Marchant, M. Edwards, G. Mercer (Eds.), Proceedings of the 2008 MISG, 2009.
[3] W. Yuen, Transient temperature distribution in a multilayer medium subject to radiative surface cooling, Applied Mathematical Modelling 18 (1994) 93–100.
[4] N. Aguirre, G. De La Cruz, Y. Gurevich, G. Logvinov, M. Kasyanchuk, Heat diffusion in two-layer structures: photoacoustic experiments, Physica Status Solidi (B) 220 (2000) 781–787.
[5] Y. Gurevich, I. Lashkevich, G. de la Cruz, Effective thermal parameters of layered films: an application to pulsed photothermal techniques, International Journal of Heat and Mass Transfer 52 (19–20) (2009) 4302–4307.
[6] J. Diard, N. Glandut, C. Montella, J. Sanchez, One layer, two layers, etc. an introduction to the EIS study of multilayer electrodes. Part 1: theory, Journal of Electro—Analytical Chemistry 578 (2005) 247–257.
[7] V. Freger, Diffusion impedance and equivalent circuit of a multilayer film, Electro—Chemistry Communications 7 (2005) 957–961.
[8] P. Grossel, F. Depasse, Alternating heat diffusion in thermophysical depth profiles: multilayer and continuous descriptions, Journal of Physics D: Applied Physics 31 (1998) 216–223.
[9] G. Liu, B. Si, Multi-layer diffusion model and error analysis applied to chamber-based gas fluxes measurements, Agricultural and Forest Meteorology 149 (2009) 169–178.
[10] G. Pontrelli, F. de Monte, Mass diffusion through two-layer porous media: an application to the drug-eluting stent, International Journal of Heat and Mass Transfer 50 (2007) 3658–3669.
[11] F. Martelli, A. Sassaroli, S.D. Bianco, G. Zaccanti, Solution of the time-dependent diffusion equation for a three-layer medium: application to study photon migration through a simplified adult head model, Physics in Medicine and Biology 52 (2007) 2827–2843.
[12] S. Gilbert, R. Mathias, Analysis of diffusion delay in a layered medium, Biophysical Journal 54 (1988) 603–610.
[13] G. Smith, Numerical Solution of Partial Differential Equations: Finite Difference Methods, second ed., Oxford University Press, 1978.
[14] O. Iliev, A finite-difference scheme of second-order accuracy for elliptic equations with discontinuous coefficients, Differential Equations 36 (6) (2000) 928–930.
[15] A. Wiegmann, K. Bube, The explicit-jump immersed interface method: finite difference methods for PDEs with piecewise smooth solutions, SIAM Journal on Numerical Analysis 37 (3) (2000) 827–862.
[16] C. Xue, S. Deng, An upwinding boundary condition capturing method for Maxwell's equations in media with material interfaces, Journal of Computational Physics 225 (2007) 342–362.
[17] W. Wang, A jump condition capturing finite difference scheme for elliptic interface problems, SIAM Journal on Scientific Computing 25 (5) (2004) 1479–1496.
[18] R. Hickson, S. Barry, G. Mercer, Critical times in multilayer diffusion. Part 1: exact solutions, International Journal of Heat and Mass Transfer 52 (25–26) (2009) 5776–5783.
[19] H. Carslaw, J. Jaeger, Conduction of Heat in Solids, second ed., Oxford University Press, Amen House, London, 1959.
[20] Maplesoft. Maple 11, Waterloo, Ontario. http://www.maplesoft.com/.
[21] R. Hickson, S. Barry, G. Mercer, Exact and numerical solutions for effective diffusivity and time lag through multiple layers, ANZIAM Journal(E) 49 (2009) C324–C340.
[22] R. Hickson, S. Barry, H. Sidhu, Critical times in one- and two-layered diffusion, Australian Journal of Engineering Education 15 (2) (2009) 77–84.
[23] K. Chang, U. Payne, Analytical and numerical approaches for heat conduction in composite materials, Mathematical and Computer Modelling 14 (1990) 899–904.
[24] P. Johnston, Diffusion in composite media: solution with simple eigenvalues and eigenfunctions, Mathematical and Computer Modelling 15 (10) (1991) 115–123.
[25] F. de Monte, Multi-layer transient heat conduction using transition time scales, International Journal of Thermal Sciences 45 (2006) 882–892.
[26] G. Oturanc, A. Sahin, Eigenvalue analysis of temperature distribution in composite walls, International Journal of Energy Research 25 (2001) 1189–1196.
[27] The MathWorks Inc. MATLAB®, Natick, Massachusetts. Version 7.5.0.338 (R2007b). http://www.mathworks.com/products/matlab/.
[28] PDE Solutions Inc. FlexPDE, Spokane Valley. Version 5. http://www.pdesolutions.com.
[29] R. Hickson, S. Barry, G. Mercer, Critical times in multilayer diffusion. Part 2: approximate solutions, International Journal of Heat and Mass Transfer 52 (25–26) (2009) 5784–5791.
[30] R. Hickson, S. Barry, H. Sidhu, G. Mercer, Critical times in single-layer reaction diffusion, International Journal of Heat and Mass Transfer, January 2011 (in press).

[31] R. Hickson, Critical times of heat and mass transport through multiple layers, Ph.D. Thesis, PEMS, UNSW@ADFA, 2010. Available at: http://unsworks.unsw.edu.au/vital/access/manager/Repository/unsworks:8938.
[32] K. Landman, M. McGuinness, Mean action time for diffusive processes, Journal of Applied Mathematics and Decision Sciences 4 (2) (2000) 125–141.
[33] A. McNabb, Means action times, time lags and mean first passage times for some diffusion problems, Mathematical and Computer Modelling 18 (10) (1993) 123–129.